NASA CR- 143693

N75-22235

TECHNIQUES FOR CARRYING OUT RADIATIVE TRANSFER CALCULATIONS FOR THE MARTIAN ATMOSPHERIC DUST

J. R. Aronson, A. G. Emslie and P. F. Strong

Arthur D. Little, Inc.
Acorn Park
Cambridge, Massachusetts 02140

September 1974

Final Report for Period June 1973 - September 1974

NASA Contract No. NAS5-23257

Prepared for

GODDARD SPACE FLIGHT CENTER
Greenbelt, Maryland 20771

Arthur D. Little, Inc.

TABLE OF CONTENTS

	ABSTRACT	ii
I.	INTRODUCTION	1
II.	THEORETICAL METHOD	3
III.	OPTICAL CONSTANTS OF MINERALS	7
IV.	MODELING THE MARTIAN DUST	21
V.	DETERMINATION OF K(ν), S(ν) AND SCALE HEIGHT H OF THE DUST CLOUD BY INVERSION OF OBSERVED DATA	30
	1. INTRODUCTION	30
	2. DETERMINATION OF S AND K IN SPECTRA REGIONS HAVING NEGLIGIBLE GAS ABSORPTION	31
	3. DETERMINATION OF S AND K IN THE PRESENCE OF GAS ABSORPTION	35
	4. DETERMINATION OF K(ν) WHEN S(ν) IS SMALL	38
	5. COMPUTER PROGRAMS	44
	APPENDIX	47
	REFERENCES	57

Abstract

This report describes the modification of a new theory of the reflectance of particulate media so as to apply it to analysis of the infrared spectra obtained by the IRIS instrument on Mariner 9. With the aid of this theory and the optical constants of muscovite mica, quartz, andesite, anorthosite, diopside pyroxenite, and dunite, we have made modeling calculations so as to refine previous estimates of the mineralogical composition of the Martian dust particles. These calculations suggest that a feldspar rich mixture is a very likely composition for the dust particles. The optical constants used for anorthosite and diopside pyroxenite were derived during this program from reflectance measurements made by F. Blaine of NASA Goddard Space Flight Center. Those for the mica were derived from literature reflectance data. Finally, a computer program was written to invert the measured radiance data so as to obtain the absorption coefficient spectrum which should then be independent of the temperature profile and gaseous component effects.

I. INTRODUCTION

The infrared spectra obtained by the IRIS experiment on Mariner 9 contain extensive data concerning the extraordinary dust storm raging on Mars at the beginning of the encounter. The principal features arising from the dust are rather broad diffuse bands centered near 480 cm^{-1} and 1085 cm^{-1}. Such bands are commonly observed in silicate minerals and represent the Si-O bending and stretching vibrations, respectively. Their precise shapes and locations provide information concerning the mineral composition and particle size distribution of the dust cloud. However, owing to the rather featureless bands, it has been difficult to interpret the spectra of the dust in very specific ways. Comparisons with Mie theory calculations for quartz[1] suggest particle diameters between 2 and 20 μm and the location of the Si-O stretching band permits the SiO_2 content of the dust to be estimated as 60 ±10%.[2] Hunt, et al.,[3] suggest the clay mineral montmorillonite as a major component of the Martian dust cloud. They base this conclusion on the comparison of the Mariner radiance data with laboratory transmission spectra in which montmorillonite shows two rather broad bands at approximately the correct positions and lacks other strong features in the mid-infrared. While other published spectra of montmorillonite are somewhat different in these respects,[4,5,6] we believe that a proper comparison requires that either radiance, transmission or absorption coefficients be compared for laboratory data and the Martian experiment to eliminate shifts and other changes caused by the physical conditions of the measurement. For instance, it is well known that the bands in reflectance spectra are often shifted to longer wavelengths with respect to their counterparts in transmittance spectra owing to the influence of the real part of the refractive index.

As the dust particles are unlikely to be spherically shaped, the Mie theory may not be strictly applicable. The authors have developed a theory of scattering by particulate media where the particles may be arbitrarily shaped.[7,8] During this contract, our theory has been

modified to apply to atmospheric particles[9] rather than those packed together on the ground. The revised theory has then been used together with the optical constants of typical candidate minerals and rocks to model the radiance spectrum of Mars. As literature values of the optical constants are scarce for mineral species, we have applied classical dispersion theory to measured spectra of muscovite mica, diopside pyroxenite and anorthosite so as to be able to adequately cover the possible range of structural types for silicate minerals. The anorthosite and diopside pyroxenite are, of course, rocks rather than minerals but are representative of essentially single mineral species.

Finally, we have written computer programs to invert the Martian radiance data with the aid of the known (CO_2 band derived) atmospheric temperature profile so as to be able to derive an absorption coefficient for the Martian dust that is free of the temperature profile and the Martian gas absorption. Such absorption coefficient spectra are perhaps the best vehicles for making detailed comparisons between the Mariner data and laboratory spectra.

II. THEORETICAL METHOD

To calculate the spectral radiance of the dust cloud on Mars for any proposed mixture of mineral particles one must first derive the scattering and absorption cross-sections of the individual particles, then compute the scattering and absorption coefficients of the particulate medium, and finally apply a radiative transfer method to determine the radiance of the cloud as a function of frequency.

To calculate the cross-sections of a particle of a given candidate mineral, we use modified geometrical optics for wavelengths small compared with the particle size (coarse particle theory), and modified Rayleigh theory for wavelengths large compared with the particle size (fine particle theory).

In the coarse particle theory we consider the particle to be a polyhedron but treat the edges of the facets of the polyhedron as though they were perturbations of the smooth surface of a sphere of the same volume as the actual particle. Therefore, we first calculate the scattering and absorption by the smooth sphere by ray tracing and then adjust the results to take account of the effect of the edges. We do this by regarding each edge as an elongated ellipsoid of particle material adhering to the sphere. We allow the ellipsoids to have a wide range of cross-sectional shapes and calculate their effect statistically. It is found that edges treated in this way can cause a large increase in the absorption, notably in strong reststrahlen bands.[7,8,9] Some of the concepts presented in these references such as the contact factor and the discrete layer model apply to packed mineral powders and are, of course, omitted in the present application to a dilute suspension of particles in an atmosphere. We also omit here the diffuse reflection from surface asperities on the particle and consider only the Fresnel reflection from a smooth surface. In the case of thin mica flakes, where the perturbed sphere is clearly not a good approximation to the particle shape, we do the ray tracing directly and average over all orientations of the flake. This removes any refractive scattering

from these calculations. It can be shown[10] that the average geometrical cross-section of any convex randomized particle is the total surface area of the particle divided by 4. The average slant path t through a particle ignoring refraction is given, therefore, by

$$t = \frac{V}{S/4} \tag{1}$$

where V is the volume and S the surface area of the particle. For the case of a disk of diameter D and thickness H, (1) becomes

$$t = \frac{2DH}{D + 2H} \cdot \tag{2}$$

Allowing for refraction, the average path can be shown to be approximately

$$t' = \frac{Hnt}{\sqrt{n^2t^2 - t^2 + H^2}} \tag{3}$$

where n is the refractive index. In our computer program we have arbitrarily chosen an aspect ratio D/H = 5/1 for mica flakes. Equation (3) then becomes

$$t' = \frac{2Dn}{\sqrt{100n^2 - 51}} \cdot \tag{4}$$

In the fine particle theory where the wavelength is large compared with the particle size, the edges of the particle become much less important than the general shape of the particle. We therefore represent an arbitrary particle by a smooth ellipsoid. Since the particles may have a wide variety of shapes, we allow the ellipsoids to vary considerably in their axial ratios. For our purpose it is most useful to specify an ellipsoid by its depolarization factors L, M and N, whose sum is 4π, since these factors cause widely differing absorption even in particles of the same volume. The average power absorbed by a randomly oriented

ellipsoid of volume V and complex index m, placed in an electric field E with angular frequency ω, is[7]

$$W = -\frac{\omega V|E|^2}{6} \underline{\text{Im}} \ (m^2 - 1) \left[\frac{1}{4\pi + L(m^2 - 1)} + \frac{1}{4\pi + M(m^2 - 1)} + \frac{1}{4\pi + N(m^2 - 1)} \right] \quad (5$$

where Im means "imaginary part of."

This expression demonstrates clearly that, as stated above, the absorbed power is not independent of the shape of the small particle, as is often assumed. Independence of shape is true only when $|m^2 - 1| \ll 1$, which is certainly not the case for a strong reststrahlen band. In such a region of the spectrum m can have values that approach the poles of the expression in square brackets in (5). For a sphere, $L=M=N=4\pi/3$, and there is therefore a single pole in m-space on the imaginary axis at the point $m = -i\sqrt{2}$. In a strong reststrahlen band the trajectory of m in m-space, as frequency is changed, runs almost parallel to the imaginary axis, and slightly displaced from it. In the case of a sphere, the pole at $-i\sqrt{2}$ therefore produces a sharp absorption peak. On the other hand, for a distribution of ellipsoidal particles with a continuous range of values L,M,N (subject to $L+M+N = 4\pi$), a continuous distribution of poles will be spread along the imaginary axis in m-space. The trajectory of m therefore remains close to poles over a considerable portion of the trajectory, thereby giving rise to a broad absorption maximum.

On averaging Equation (5) over all allowable combinations of L,M,N, one finds[9] for the average absorption cross-section of small particles with a wide variety of shapes

$$\sigma_a = \frac{2\pi^2 \nu d^3}{3} \underline{\text{Im}} \left(-\frac{m^2 \ell n m^2}{m^2 - 1} \right) \quad (6$$

where ν is the frequency in cm^{-1} and $\pi d^3/6 = V$. It is found that this expression does indeed give a broad absorption band in a strong reststrahlen region, while a Mie theory calculation for spheres[1] of the same volume V gives a sharp absorption band.

It is worth noting that the validity of expressions (5) and (6) demands a more stringent requirement on the particle size d than the criteria $\pi d/\lambda \ll 1$ and $|m|\pi d/\lambda \ll 1$ given by van de Hulst[10] for the Rayleigh region. The additional restriction is clearly related to the minimum separation of the m-trajectory from the imaginary axis, but has not been formulated owing to the lack of an explicit exact theory for ellipsoids.

Reference 9 also gives an expression for the average scattering cross-section for the distribution of small ellipsoidal particles.

The absorption mechanism just discussed acts also at the edges of large particles, regarded as elongated ellipsoids, and is responsible for the enhanced absorption mentioned earlier with respect to the coarse-particle theory.

In the intermediate range of wavelengths where $\lambda \sim d$, we estimate the cross-sections by means of a suitable bridging formula[9] that gives a weighted average of the results from the fine and coarse particle theories in such a way that the two theories merge slowly.

The radiative transfer method by which the radiance of the dust cloud is calculated is based on a six-stream model, also used by Conel,[11] with three upward-directed streams and three downward-directed streams, all inclined at an angle of $\cos^{-1}(1/\sqrt{3})$ to the vertical. Additional programs were written to carry out the calculation of a brightness temperature based on the radiance obtained from an arbitrary number of isothermal layers for a dust cloud, treating the ground as a blackbody. We assume that the dust cloud varies with height Z only with respect to concentration N (particles/cm^3) and not with respect to particle size distribution or mixing ratios of different minerals. The details are given in Reference 9.

III. OPTICAL CONSTANTS OF MINERALS

In order to model the radiance spectrum of the Martian dust, it is necessary to have information on the complex refractive index, $m = n - i\,k$, of the candidate species over the spectral range involved. As such data has long been available for quartz,[12] this mineral is commonly used for model calculations despite the fact that it represents an extreme in the behavior of silicate minerals. The literature data[12] is particularly useful as it is given in the form of classical dispersion theory parameters so that the optical constants at any point in the infrared can be calculated when needed from a small set of oscillator parameters.

Recently, Pollack, et al.,[13] have published similar parameters for basalt and andesite rocks. The difficulty with using such data for rocks is that in addition to the usual problem of orientation of the crystallites common to any microcrystalline material, rocks are generally mixtures of variable composition. Therefore, any such parameters would be appropriate only for the particular rock used in the measurement. However, Prof. Frondel of the Harvard geology department informs us that the composition of andesites are not as exceesively variable as for many other rocks. Andesite consists principally of oligoclase or andesine feldspar but other minerals are frequently present.

There are however, some rocks of almost single mineral composition. They include dunite, anorthosite and pyroxenite. We believe it is worthwhile to model using optical constants for such rocks as they represent structural types and the only significant variations (beside anisotropy) are in the cation ratios. It is well known[14] that the Si-O stretching frequency correlates with structural type. Such modeling amounts to disregarding the anisotropy involved, on the basis that it would always be approximately the same for natural unoriented samples. A further reason for the use of essentially monominerallic rocks as opposed to single crystals of minerals is that it is often hard to obtain suitable mineral

samples for analysis and that, in general, three sets of optical constants would be required for each single crystal corresponding to the three principal mineral orientations.

Optical constants for dunite (olivine) calculated by R. Vincent were obtained from R. Curran of NASA Goddard Space Flight Center. A sample of anorthosite from Essex County, New York, was obtained from Ward's Natural Science Establishment. Prof. Frondel of Harvard University examined our sample and noted that some crystallites were rather large so that averaging might be necessary. Anorthosites consist largely of feldspar anorthite which is the calcium-rich end member of the plagioclase feldspar minerals. Our polycrystalline sample was polished for reflectance measurements on three sides. The plan was that any orientation effects caused by large non-random crystals within our sample could be examined and might be averaged out. In addition, a microcrystalline diopside pyroxenite rock, which is essentially pure diopside, was obtained from Prof. Frondel and polished for a similar analysis.

The reflectance measurements were made by F. Blaine of NASA Goddard Space Flight Center. A wire grid infrared polarizer was used to ascertain whether significant polarization effects exist. After examining the measurements made both with and without the polarizer for the pyroxenite and anorthosite, we chose suitable spectra for reduction to the optical constants.

The optical constants of muscovite mica have been obtained from the published data of Vedder.[15] As the author no longer has the concomitant data on the refractive index, we used his recorded measurements, together with Blaine's measurements for the anorthosite and pyroxenite rocks to produce classical oscillator parameters for use in our modeling calculations. For the two rock samples a set of averaged optical constants was produced while for mica three sets of optical constants for the E||a, E||b,

and E⊥a,b orientations were obtained. The E⊥a,b is very close to an E∥c orientation so that the three possible sets of optical constants for this mineral are now available.

The computer program used to generate the optical constants from reflectance data in terms of classical oscillator parameters (Lorentz lines) is similar to one previously used for garnet and glass.[16] The old program has been modified to greatly improve the convergence rate, and a statistical section has been added at the end to calculate the standard deviations of the Lorentz line parameters. A detailed discussion of the method of regression is given in the Appendix.

Tables 1-5 show the Lorentz line parameters and their estimated standard deviations, σ, obtained by fitting the measured reflection spectra. The formula for the dielectric constant in terms of the tabulated parameters is

$$\varepsilon = \varepsilon_0 + \sum_j \frac{S_j}{1 + i\gamma_j \frac{\nu}{\nu_j} \left(\frac{\nu}{\nu_j}\right)^2} \qquad (7)$$

where S_j is the line strength, γ_j the damping and ν_j the frequency for each resonance, j. ε_0 is the high frequency dielectric constant.

Figures 1-5 show the measured spectral data (plotted as points) and the theoretical spectrum for comparison. It is of course possible to improve the fits still further by the addition of additional resonances, but we believe that the experimental data does not warrant additional effort. We recognize that a truly rigorous set of averaged optical constants for rock species cannot be obtained in this way in view of orientation-polarization effects, the imperfect nature of the surfaces and the approximation involved in averaging reflectances rather than cross-sections. Nonetheless, we believe that the set of pseudo-optical constants obtained here for monomineralic rocks are entirely adequate to

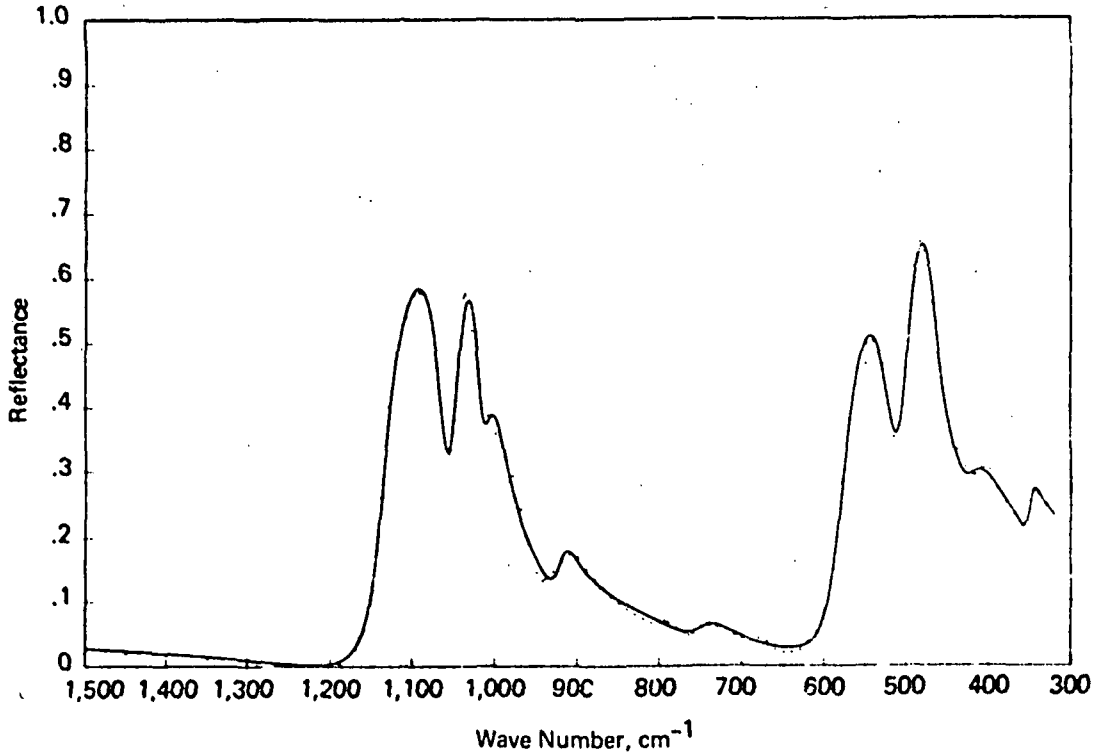

FIGURE 1 LORENTZ LINE PARAMETER FIT TO MUSCOVITA MICA, Ella

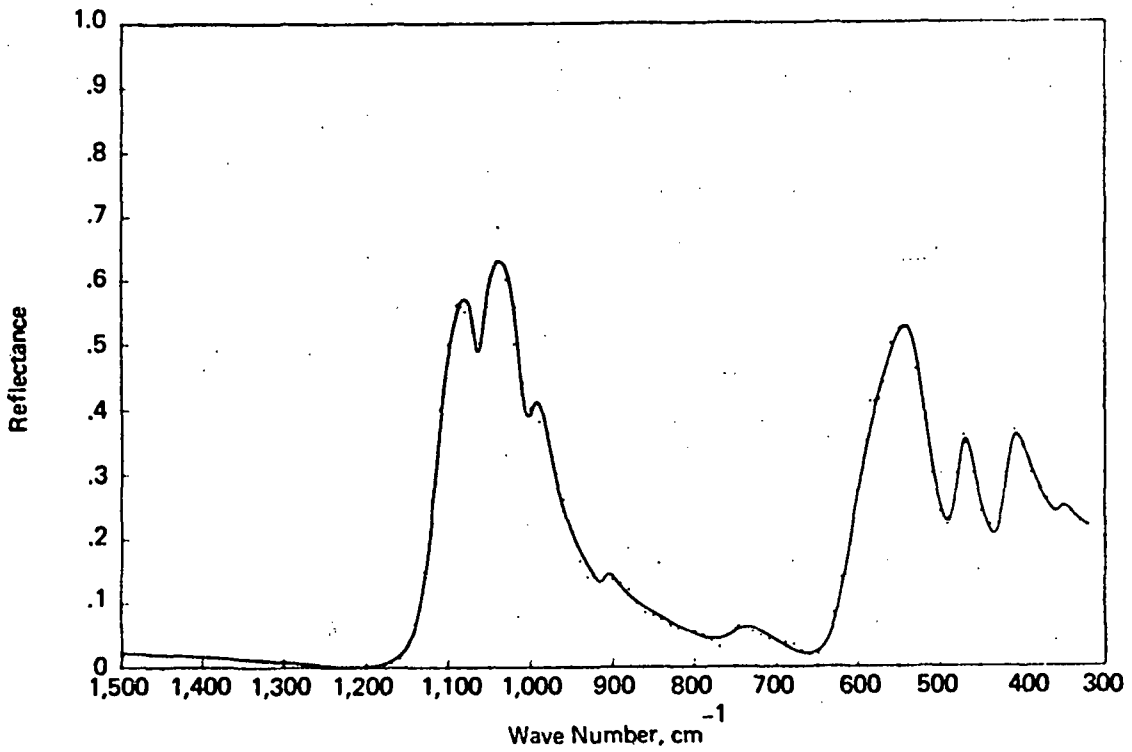

FIGURE 2 LORENTZ LINE PARAMETER FIT TO MUSCOVITE MICA, Ellb

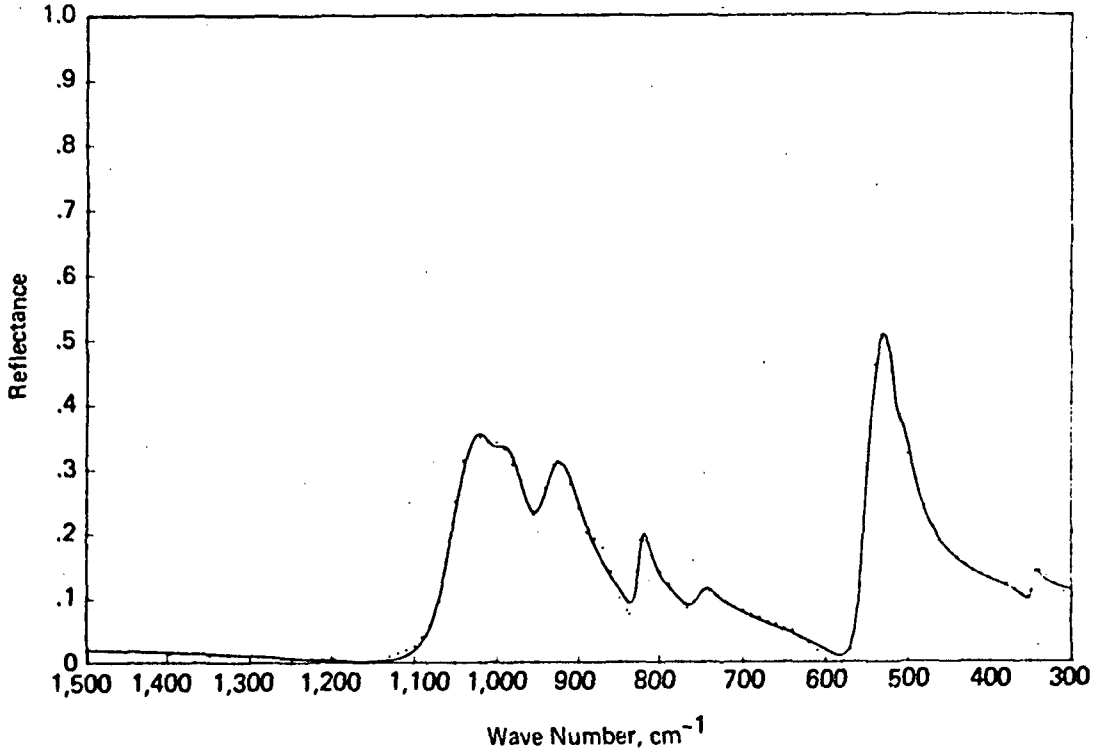

FIGURE 3 LORENTZ LINE PARAMETER FIT TO MUSCOVITA MICA, E⊥a, b

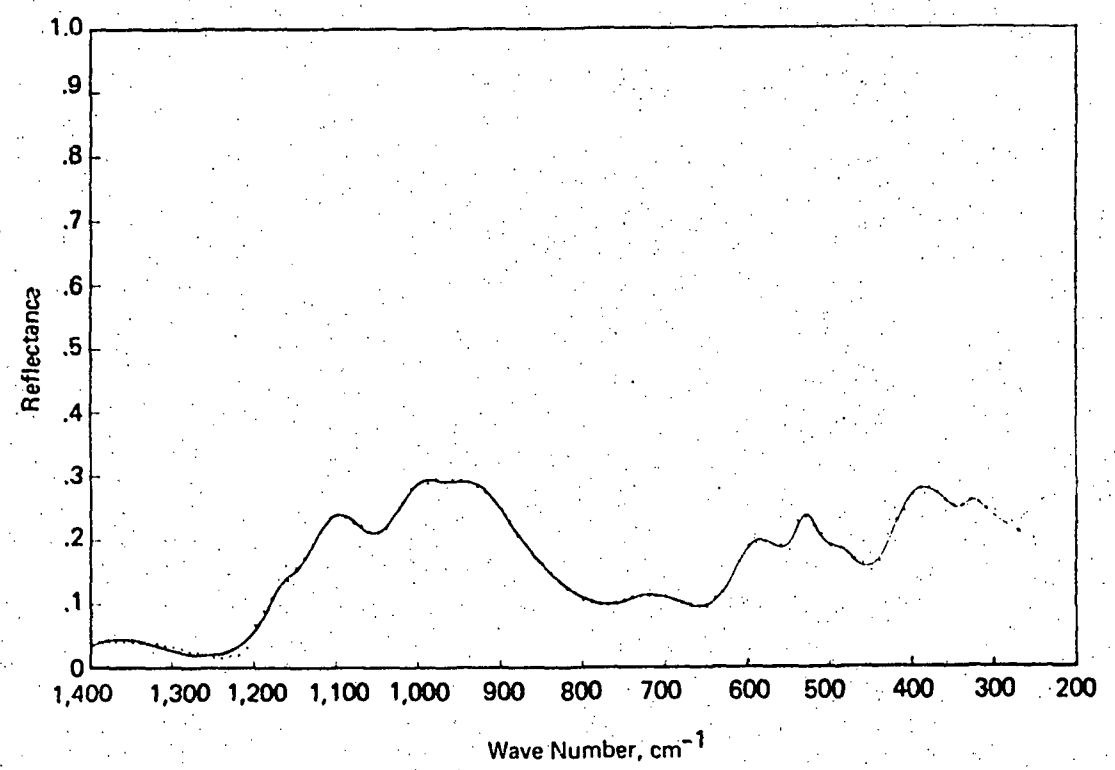

FIGURE 4 LORENTZ LINE PARAMETER FIT TO ANORTHOSITE

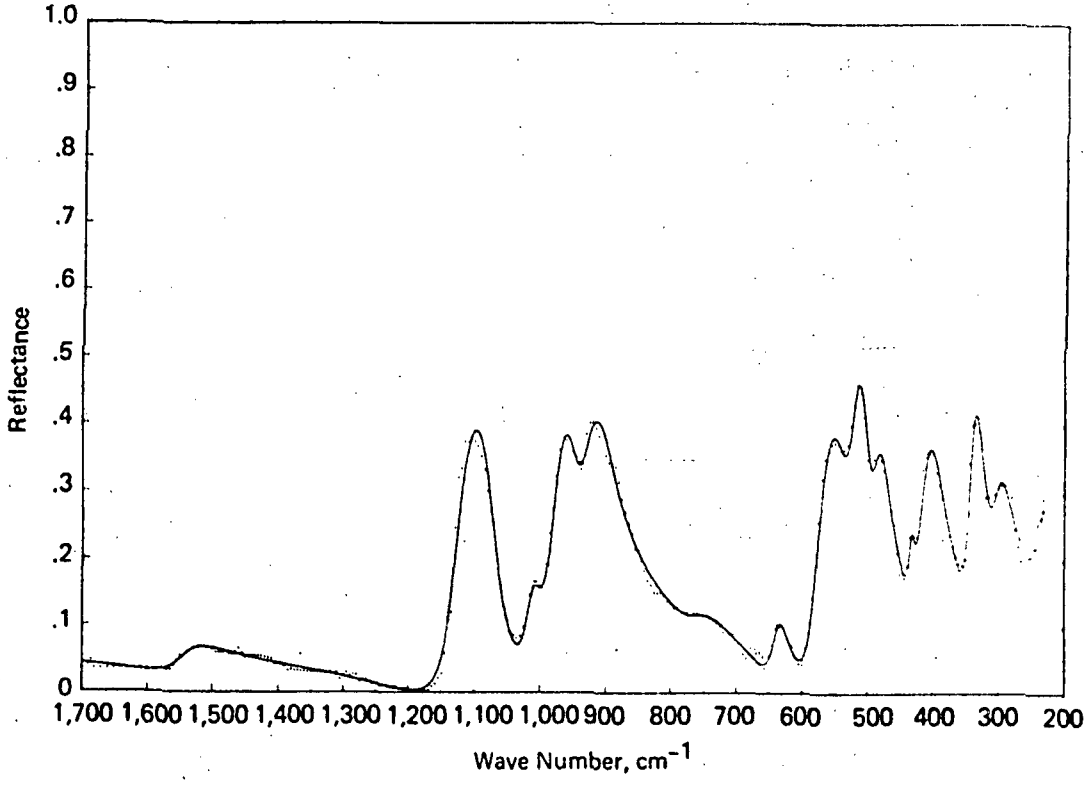

FIGURE 5 LORENTZ LINE PARAMETER FIT TO DIOPSIDE PYROXENITE

characterize the structural type represented by the spectral data for the Martian dust.

j	ν_j	$\sigma(\nu_j)$	γ_j	$\sigma(\gamma_j)$	S_j	$\sigma(S_j)$
1	1066.7	0.5	0.0258	0.0012	0.078	0.007
2	1023.4	0.7	0.0173	0.0014	0.144	0.021
3	999.9	1.3	0.0299	0.0029	0.288	0.026
4	917.7	2.1	0.0318	0.0075	0.069	0.015
5	743.4	7.2	0.0632	0.0401	0.038	0.027
6	647.0	29.1	0.2667	0.1280	0.114	0.061
7	525.4	0.6	0.0705	0.0034	0.366	0.027
8	471.2	0.6	0.0412	0.0019	1.214	0.045
9	416.4	2.6	0.1047	0.0224	0.401	0.084
10	348.6	1.3	0.0440	0.0144	0.137	0.039

$\varepsilon_0 = 2.713 \qquad \sigma(\varepsilon_0) = 0.057$

TABLE 1. Lorentz line parameters for Mica, E||a.

Range of validity is $320 \leq \nu \leq 1500$ cm^{-1}.

j	ν_j	$\sigma(\nu_j)$	γ_j	$\sigma(\gamma_j)$	S_j	$\sigma(S_j)$
1	1067.2	.9	.0182	.0035	.011	.002
2	1015.6	1.0	.0234	.0021	.168	.030
3	987.6	1.5	.0311	.0032	.325	.030
4	908.7	3.7	.0190	.0241	.017	.014
5	744.2	6.4	.0853	.0296	.073	.022
6	559.3	23.3	.1919	.0427	.236	.177
7	527.6	1.0	.0593	.0075	.711	.114
8	470.1	1.0	.0527	.0058	.404	.042
9	409.7	1.2	.0759	.0081	.697	.058
10	353.5	6.8	.0553	.0464	.068	.054

$\varepsilon_0 = 2.553 \quad \sigma(\varepsilon_0) = 0.071$

TABLE 2. Lorentz line parameters for Mica, E||b.

Range of validity is $320 \leq \nu \leq 1500$ cm^{-1}.

j	ν_j	$\sigma(\nu_j)$	γ_j	$\sigma(\gamma_j)$	S_j	$\sigma(S_j)$
1	1008.0	3.8	.0393	.0093	.021	.012
2	972.7	1.3	.0507	.0061	.150	.029
3	915.7	1.2	.0519	.0034	.324	.018
4	821.8	.7	.0206	.0018	.067	.006
5	752.2	2.6	.0358	.0092	.036	.009
6	519.5	.8	.0332	.0039	.207	.053
7	505.9	1.3	.0512	.0036	.425	.060
8	347.3	1.5	.0313	.0142	.042	.010

$\varepsilon_0 = 2.243 \qquad \sigma(\varepsilon_0) = 0.038$

TABLE 3. Lorentz line parameters for Mica, E$\perp$a and b.
Range of validity is $300 \leq \nu \leq 1500$ cm^{-1}.

j	ν_j	$\sigma(\nu_j)$	γ_j	$\sigma(\gamma_j)$	S_j	$\sigma(S_j)$
1	1352.2	8.3	.1101	.0121	.088	.012
2	1155.8	3.4	.0458	.0142	.010	.005
3	1076.1	2.8	.0873	.0092	.110	.023
4	979.3	6.7	.1018	.0239	.183	.132
5	918.4	3.9	.1060	.0179	.517	.120
6	723.2	3.9	.1715	.0247	.221	.037
7	585.7	2.5	.1462	.0143	.408	.058
8	528.9	1.7	.0705	.0134	.198	.055
9	491.3	5.2	.0981	.0379	.125	.060
10	392.7	1.9	.2232	.0164	1.292	.103
11	330.5	2.7	.1036	.0330	.186	.073

$\epsilon_0 = 2.147 \quad \sigma(\epsilon_0) = 0.163$

TABLE 4. Lorentz line parameters for anorthosite (average of three spectra). Range of validity is $250 \leq \nu \leq 1400$ cm^{-1}.

j	ν_j	$\sigma(\nu_j)$	γ_j	$\sigma(\gamma_j)$	S_j	$\sigma(S_j)$
1	1536.4	5.4	.0559	.0127	.052	.010
2	1077.2	.6	.0324	.0008	.151	.005
3	1006.8	1.2	.0326	.0048	.032	.005
4	951.3	1.1	.0386	.0040	.113	.020
5	904.5	1.1	.0532	.0036	.545	.026
6	755.9	5.8	.0956	.0271	.080	.021
7	634.8	1.8	.0469	.0068	.066	.008
8	542.1	1.2	.0814	.0048	.269	.036
9	507.3	.7	.0441	.0050	.345	.053
10	480.0	1.2	.0599	.0069	.439	.049
11	433.6	1.0	.0236	.0073	.039	.013
12	401.5	1.4	.0875	.0059	.754	.029
13	333.1	1.1	.0579	.0037	.584	.074
14	297.9	1.7	.1063	.0241	.572	.138
15	186.3	22.7	.3096	.0920	6.126	4.026

$\varepsilon_0 = 3.2358 \quad \sigma(\varepsilon_0) = 0.063$

TABLE 5. Lorentz line parameters for pyroxenite.
Range of validity is $230 \leq \nu \leq 1700$ cm^{-1}.

IV. MODELING THE MARTIAN DUST

We have used the optical constants for the various minerals and rocks together with our theory of particulate scattering to model the observed infrared spectra obtained during the Martian dust storm. For this purpose an averaged spectrum was obtained from Dr. Conrath, together with the relevant temperature profile. This profile consists of 19 atmospheric layer heights and associated temperatures, a scale height derived from the 15 μ carbon dioxide band, and a blackbody temperature for the ground. We used a linear interpolation of the temperature data to get an average temperature for each layer so that we actually used 18 atmospheric layers in our program. Some of the modeling calculations had previously been run with an 8 atmospheric layer profile taken[2] from the revolution 20 and the spectral shape differences between the two profiles are minor.

A set of computed spectra for quartz as a function of particle size is shown in Figure 6 together with the Martian dust. This set illustrates the trend to feature broadening as the particle size is increased, which has also been observed in Mie scattering calculations.[1] This trend appears to be quite general and indicates the approximate particle size by the breadth of the Si-O stretching band. We treat quartz as if it were randomly oriented so that we always take a 2:1 ratio for the $E\perp c : E\parallel c$ particle densities. For submicron particles, our calculations, which are in this case based on Rayleigh scattering by a distribution of elliptical particles, clearly indicate that the sharpening no longer occurs. The absorption coefficient decreases with Nd^3 and the scattering coefficient with Nd^6, but by the time one reaches submicron sizes, the scattering is negligible compared to the absorption. Therefore, on the assumption that the volume fraction $\pi d^3 N/6$ of the particles is constant, the absorption coefficient is also constant and one can no longer estimate N and d independently from a given spectral band. We have demonstrated

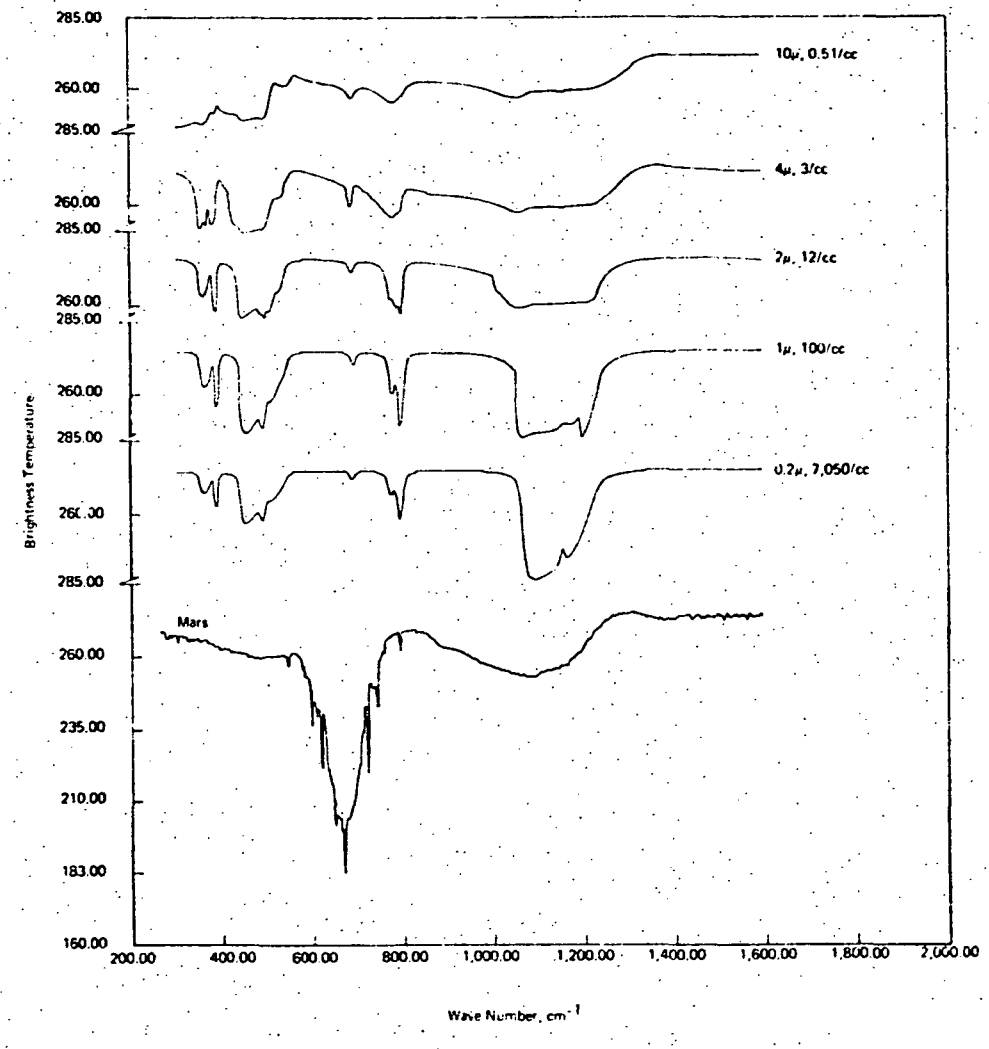

FIGURE 6 COMPUTED SPECTRA OF QUARTZ

this difficulty in several runs and believe the Mie theory would show the same results for a distribution of shapes, as it passes over to Rayleigh scattering for very small particles, if the Mie theory could be extended to such a case. Owing to the calculated breadth of our fine particle bands, other constraints must be applied to set a lower boundary on particle size if the particle size is quite small. For coarse particles, however, the broadening trend is so strong that the feldspars, which have smaller frequency dependent excursions in the optical constants, produce relatively featureless spectra at particle sizes in excess of 10 μ.

Figure 7 shows the spectra of 1 μ particles of the species that we have run (in the case of mica flakes, 4 μ diameter particles having a thickness of 0.8 μ). The general trend of the Si-O stretching bands near 10 μ with structure can be seen to run from quartz at the high frequency end through the feldspars (anorthosite and andesite), mica, and pyroxenite to dunite. This trend, as is well known, is due to the variation in silicate structure where quartz represents a complete sharing of the tetrahedral SiO_4 oxygens and the sharing is gradually reduced until in the olivine structure possessed by the dunite there is no oxygen sharing. The SiO_4 tetrahedra are, in this case, isolated by the intervening cations (mostly Mg^{++}). The trend is of a general sort, however, and individual variations within each structural type are known to cause a range of band positions that allows considerable overlap between adjacent structural types.[14]

The particle densities shown in Figure 7 were held constant. They are adjustable parameters in our computer program but their basic effect is simply to change the spectral level provided the densities are sufficient that the spectral bands may be clearly observed. The mica data was calculated for a random orientation of flakes by taking equal numbers of particles of each of the three orientations $E \| a$, $E \| b$, and $E \perp a,b$ (essentially[15] $E \| c$). We have also examined the effect of considering only

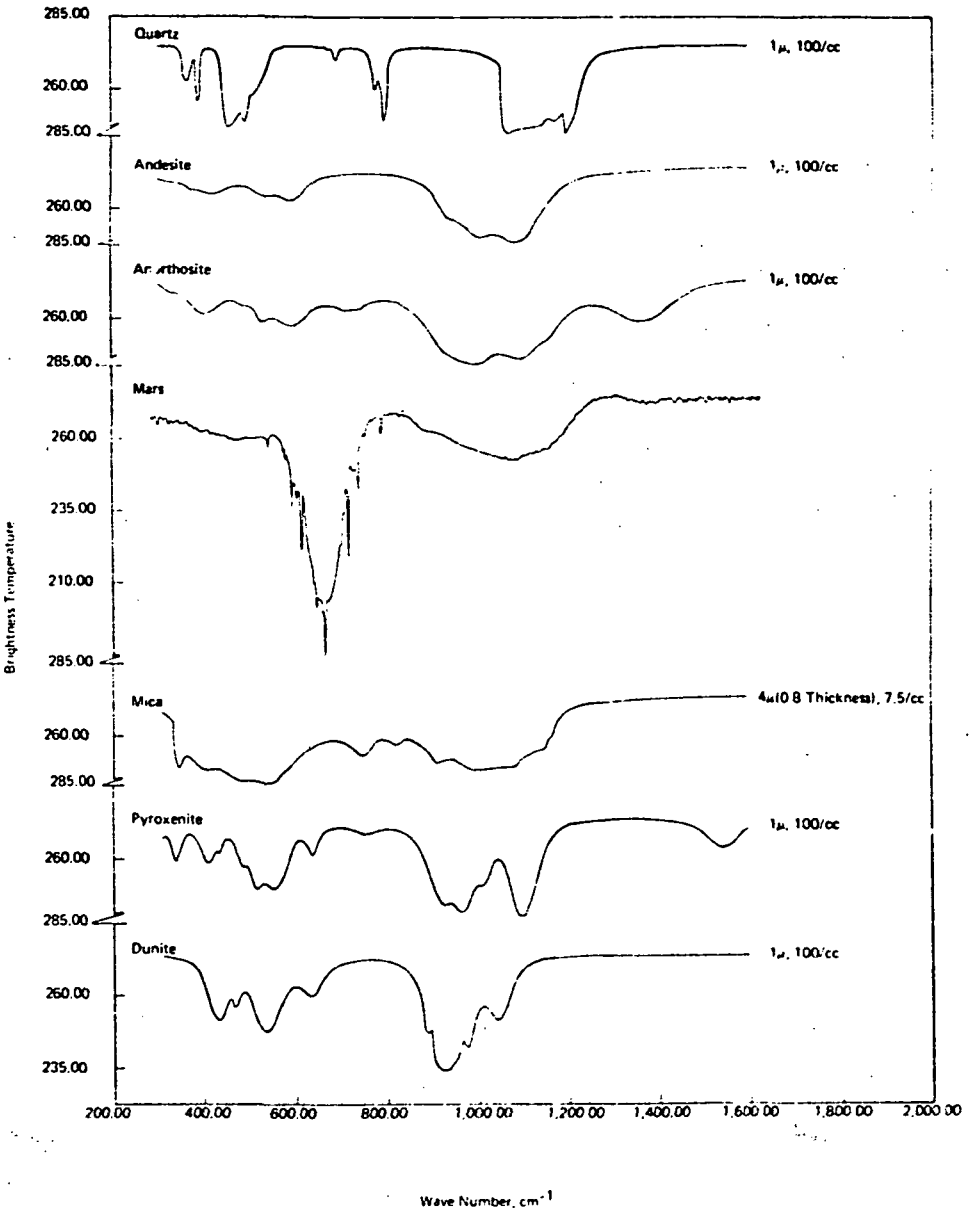

FIGURE 7 COMPUTED SPECTRA OF ROCKS AND MINERALS

the two orientations, E||a and E||b, as opposed to all three orientations in order to examine the range of differences to be expected if the particles are settling slowly with the sheets aligned parallel to the ground ather than tumbling in random fashion, although even in such a case significant amounts of the E||c orientation would be seen owing to the diffuse nature of the radiative transfer.

We chose to obtain the optical constants and run the mica data, not only to fill in the structural sequence discussed above, but as a proxy for the clay mineral montmorillonite suggested by Hunt, et al.,[3] to be a good Martian candidate. Transmission spectra published by Moenke[5] indicate that montmorillonite and muscovite have very similar spectra, which is not unexpected owing to their common sheet-like structure. Moenke shows a Si-O stretching frequency about $10cm^{-1}$ lower in muscovite than in montmorillonite, although the spectra of both species are known to be somewhat variable.[4,17,18]

As already stated, andesites are rocks of somewhat variable composition. The evidence that this high concentration feldspar containing rock had similarities to the Martian data led us originally to propose the ail feldspar rock anorthosite as a candidate species and so to develop its optical constants. The resulting spectrum gave, for the first time, to our knowledge a possible explanation of the hitherto mysterious band near 1380 cm^{-1}. However, a reexamination of the data (Figure 4) which resulted in the resonance giving rise to this feature casts some doubt on its reality. The mathematical analysis (Table 4) appears to validate the line in question, but the raw data shows the reflectance level to flatten out at still higher frequencies. Because of the low value of the reflectance and the noise characteristics of the measurements, we are hesitant to claim the reality of the 1380 cm^{-1} feature.

Examination of the data in Figure 7 indicates that the Si-O stretching band of the two feldspar containing rocks and the muscovite mica fit the

Martian data considerably better than the other species with respect to both band shape and position. The feldspars appear to have a somewhat higher stretching frequency band than the mica, as expected, and thus fit the Martian data somewhat better. However, the low frequency band near 500 cm^{-1} is another matter. For this band the mica is preferable owing to its lack of a window region in the center of the band, but contraindicated by the relative strength of the band compared to the Si-O stretching band. In the latter respect, the feldspars are preferable. Both of these characteristics might be improved on by the choice of a suitable mixture, as the attempt to model the spectrum of Mars with a single species is likely to be quite unrealistic.

The choice of 1 μ for the anorthosite size in Figure 7 was based on the band breadth behavior of a set of anorthosite spectra analogous to the quartz set given in Figure 6. The Si-O stretching band, as shown in Figure 7, is slightly less broad than in the Martian data suggesting that the particle size is slightly greater than 1 μ. Our 2 μ anorthosite results on the other hand give a broader band whose shape has been sufficiently distorted so that it no longer resembles the Martian band. Similarly, for mica (whose band position makes it also a tenable candidate) the best appearing spectrum results from a flake of thickness near 1 μ and significantly smaller particles have a distinctly narrower band.

If we restrict ourselves to single species, we feel that in view of the lack of optical constants for very many mineral species, a reasonably good fit to the Martian data is shown by both anorthosite and mica in Figure 8. Here we have simply reduced the particle densities so as to better approximate the data. While the anorthosite fit is by no means perfect, the band positions for both major bands (ignoring the 500 cm^{-1} peak in the middle of the low frequency band), their breadths and relative intensities strongly suggest a feldspar as a principal candidate for the Martian dust. The mica fit is not quite as good as discussed above.

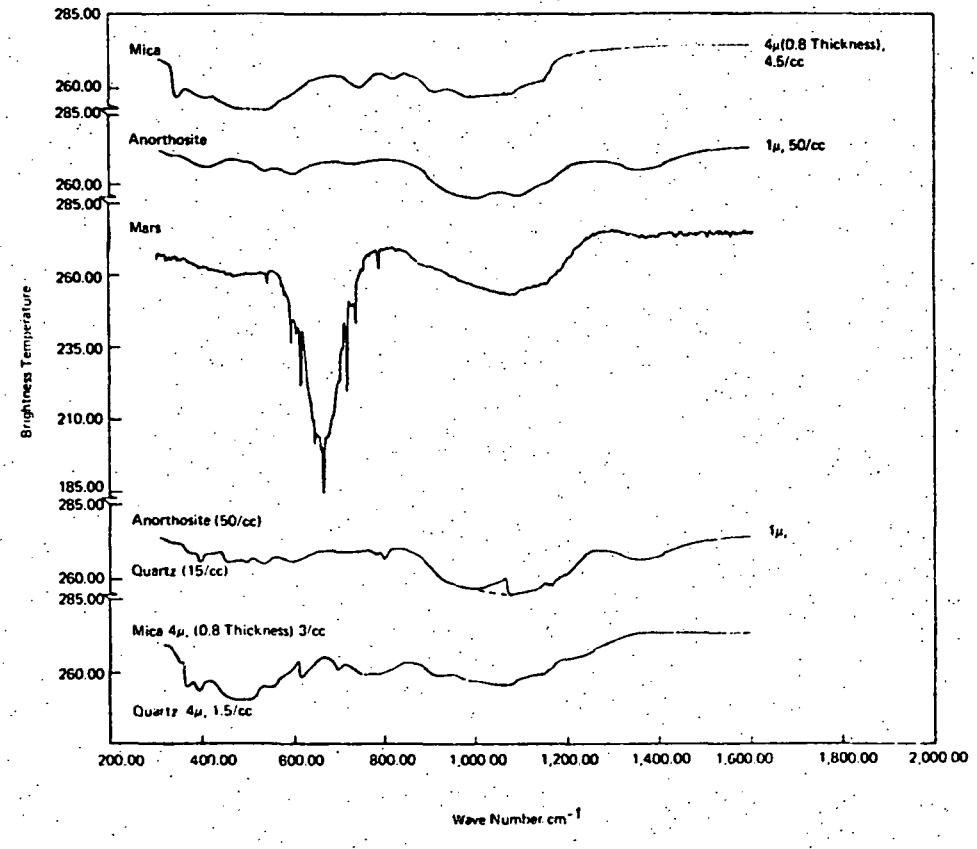

FIGURE 8 BEST FITS TO MARTIAN SPECTRUM

All the plagioclase feldspars appear to show similar spectral structure[17] to the anorthosite and, as the window in the middle of the 500 cm^{-1} band is the principal difficulty, we decided to try a mixture of anorthosite with quartz. The result of one run is shown in Figure 8. The quartz does fill the window in the 500 cm^{-1} band as well as shift the Si-O stretching band to slightly higher frequencies which is desirable, but, unfortunately, introduces a discontinuity in the Si-O stretching band. This feature is due to the use of 1 μ quartz rather than a slightly larger size (see Figure 6) to avoid a defect in our simple bridging relationship which was designed for mixing either coarse particles of several types or fine particles of several types. The defect results from bridging between the two theories for the entire mixture rather than separately for each mineral component. Judging by our various runs, the best fit should be produced by fine particle anorthosite and somewhat coarser particle quartz. We have dashed in the expected result of such reprogramming on the figure. As the evidence of our various runs suggested that a combination of coarse particle (4 μ) mica and quartz might also result in a better fit than the mica alone, we ran such a mix as well, and it is also included in Figure 8. It is important to note that 4 μ mica, as before, refers to the disk diameter and the thickness is taken to be 0.8 μ. The relative coarseness (4 μ) of the quartz particles is used principally to assure that the mica spectrum is not forced into the fine particle regime owing to the previously mentioned defect in our simple bridging relationship. The Si-O stretching band is better centered than for the mica alone but appears too broad. Significant additional structure in the 800 cm^{-1} region and in the 500 cm^{-1} band is created but all things considered the fit is not too bad.

In comparison to the mixture of anorthosite and quartz, the relative flatness and extra breadth of the Si-O stretching band and the intensity reversal shown compared to the two principal Martian bands (near 500 cm^{-1} and 1000 cm^{-1}) are the most significant reasons for our preference of the feldspar dominated mix. This is even discounting the somewhat uncertain 1380 cm^{-1} feature as discussed previously.

We believe that a feldspar dominated mixture containing some quartz and mica would provide a still better fit, but this would require some reprogramming of the relationship bridging our fine and coarse particle theories.

V. DETERMINATION OF K(ν), S(ν) AND SCALE HEIGHT H OF THE DUST CLOUD BY INVERSION OF OBSERVED SPECTRA

A. INTRODUCTION

At our meeting at Goddard Space Flight Center in July 1973 we suggested the possiblity that the effect of atmospheric gas absorption could be removed from the dust cloud spectra if, with the help of a simple radiative transfer theory, one suitably combined the spectra observed for two quite different temperature profiles. We have pursued this idea further and now believe that the two-temperature profile scheme, besides eliminating the effect of gas absorption, can provide spectral data directly related to the scattering and absorption cross-sections of the dust particles themselves and therefore be of greater diagnostic value than the cloud spectral radiance or brightness temperature. The parameters that can be derived by the two-temperature profile method are the scattering and absorption coefficients S(ν) and K(ν) of the dust cloud which are proportional to the scattering and absorption cross-sections of the particles, and independent of temperature distribution and gas absorption. The method requires an assumption about the scale height of the dust cloud, e.g., the same as that of the atmosphere.

In the spectral regions with negligible gas absorption the method is very simple. With gas absorption a more involved computer program is necessary. In both cases the procedure can be readily used in computer modeling, i.e., in calculating spectral radiance for given temperature profile, particle density distribution, and particle scattering and absorption cross-sections derived from our theory or the Mie theory.

The foregoing inversion scheme was worked out at a time when it was thought that the dust particles were large enough, relative to the wavelength,

that S and K would be of comparable magnitude. It has since developed, from aerodynamic considerations and the spectral evidence discussed above, that the particle size ($\sim$1 μ) is small compared with the wavelength ($\sim$10 μ). Under these conditions the effect of S on the spectral shape is too small to permit S to be determined by the two-profile method. We have therefore considered the possibility of determining the scale height H and $K(\nu)$ for the dust cloud, instead of $S(\nu)$ and $K(\nu)$, by the two-profile scheme.

B. DETERMINATION OF S AND K IN SPECTRAL REGIONS HAVING NEGLIGIBLE GAS ABSORPTION

We assume that the dust cloud varies with height Z only with respect to concentration (particles/cm^3) and not with respect to particle size distribution or mixing ratios of different minerals. Under these conditions, S and K are each proportional to concentration n(Z). The radiance of the cloud, in spectral regions with no gas absorption, is not changed if the cloud is compressed to uniform particle concentration, provided that each plane of particles retains its original temperature. The new height Z of any plane is related to the original height Z_0 by the formula

$$Z = \frac{1}{n_0} \int_0^{Z_0} n(Z_0) dZ_0 \qquad (8)$$

where n_0 is the concentration near the ground.

We represent the radiation distribution at any point in the uniform cloud by six mutually perpendicular discrete beams equally inclined to the Z-axis. From symmetry the three upward-directed beams are of equal intensity and produce a resultant flux density $I(\nu)$. The three downward-directed beams have a resultant flux density $J(\nu)$. The radiative transfer equations then have the simple form

$$\frac{dI}{dZ} = -(K + S)I + SJ + KB \tag{9}$$

$$-\frac{dJ}{dZ} = -(K + S)J + SI + KB \tag{10}$$

where $B = B(T,\nu)$ is the Planck function at any point.

Using a Green's function approach, we have solved (9) and (10) for the radiative flux N leaving the top of the cloud under the assumption that the ground is composed of the same particles as the cloud and has a uniform temperature corresponding to a Planck function $B_0(\nu)$.

The result is

$$N = (1 - R)\gamma \int_0^H B(h)e^{-\gamma h}dh + (1 - R)B_0e^{-\gamma h} \tag{11}$$

where H is the thickness of the uniform cloud and h = H-Z. The parameters R and γ are the reflectance (albedo) of a semi-infinite cloud, and the extinction coefficient of the radiation in the cloud, respectively, and are related to K and S by the formulas

$$R = 1 + \frac{K}{S} - \sqrt{\frac{K^2}{S^2} + 2\frac{K}{S}} \tag{12}$$

$$\gamma = \sqrt{K^2 + 2KS} \tag{13}$$

In practice one could divide the cloud into a number of isothermal layers as in Figure 9. Equation (11) then becomes

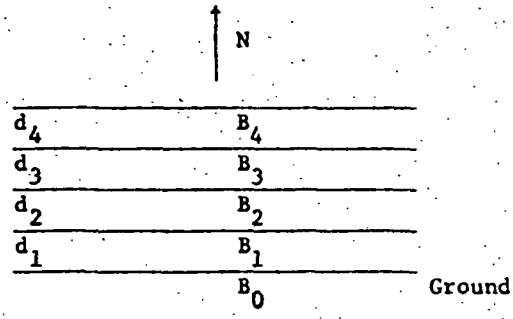

Figure 9

$$N = (1 - R)\left\{B_4 + (B_3 - B_4)e^{-\gamma d_4} + (B_2 - B_3)e^{-\gamma(d_4 + d_3)}\right.$$

$$\left. + (B_1 - B_2)e^{-\gamma(d_4 + d_3 + d_2)} + (B_0 - B_1)e^{-\gamma(d_4 + d_3 + d_2 + d_1)}\right\} \qquad (14)$$

This simple result can obviously be extended to any number of isothermal layers.

Eq (14) can be modified to replace layer thicknesses by layer heights and to treat the ground as a blackbody rather than as an isothermal semi-infinite extension of the cloud. The new equation, generalized to n layers, is

$$N = \frac{(1 - R^2)e^{-\gamma H_n} B_G}{1 - R^2 e^{-2\gamma H_n}} +$$

$$\frac{(1 - R)e^{-\gamma H_n}}{1 - R^2 e^{-2\gamma H_n}} \sum_{i=1}^{n} \left[B_i \left(e^{\gamma H_i} - e^{\gamma H_{i-1}}\right) - R\left(e^{-\gamma H_{i-1}} - e^{-\gamma H_i}\right)\right] \qquad (15)$$

where $\gamma H_o = 0$, B_G is the Planck function for the ground and the H_i represents the heights of the i layers. The calculations have been made on the assumption of an exponential dependence of particle concentration on height. As before the cloud is treated as if it were compressed to layers of equal particle density having, however, the temperatures of the original layers.

To determine R and γ from the Martian spectra, one would select two spectra with widely different temperature profiles taken closely enough in time and space so that the dust cloud can be assumed to be unchanged. For the two spectra Equation (15) can be written in the form

$$N = (1 - R)\, F(B_4, B_3, B_2, B_1, B_0, \gamma) \tag{16}$$

$$N' = (1 - R)\, F(B'_4, B'_3, B'_2, B'_1, B'_0, \gamma) \tag{17}$$

where N, N', and the B's and B' 's are known.

On dividing (16) by (17), 1 - R cancels out and we obtain an equation for γ alone. This can be solved readily by Newton's method. R can then be determined directly from Equation (16).

The scattering and absorption coefficients can be found by means of the relations

$$S = \frac{2\gamma R}{1 - R^2} \tag{18}$$

$$K = \frac{\gamma(1 - R)}{1 + R} \tag{19}$$

which one can derive from (12) and (13).

C. DETERMINATION OF S AND K IN THE PRESENCE OF GAS ABSORPTION

In spectral regions where gas absorption is significant, K/S is, in general, no longer independent of Z since the absorption coefficients of the gas and dust do not vary in the same way with Z. The simple solution (11) therefore does not apply. We may, however, make the dust cloud uniform as before by the Z-transformation (8). At the same time we must similarly adjust the gas absorption coefficient from $K_g(Z_0)$ to $K_g(Z)$ by the formula

$$K_g(Z) = \frac{n_0}{n(Z_0)} \cdot K_g(Z_0) \tag{20}$$

Next we divide the cloud into a number of isothermal layers as before. In any given isothermal layer, the general solution of (9) and (10) is

$$I = Ae^{-\gamma Z} + Ce^{\gamma Z} + B \tag{21}$$

$$J = RAe^{-\gamma Z} + \frac{1}{R}Ce^{\gamma Z} + B \tag{22}$$

where A and C are arbitrary constants to be determined by the boundary conditions of continuity of I and J at each interface. At the top of the cloud J = 0 and we assume now that the ground has an arbitrary emissivity $\varepsilon(\nu)$. For the case of the four-layer subdivision shown in Figure 10, we have eight arbitrary constants, A_1, C_1, A_2, C_2, A_3, C_3, A_4, C_4 and eight equations derived from the boundary conditions. These simultaneous equations are displayed in Table 6. It is clear how the matrix can be extended to the case of more layers.

TABLE 6

Simultaneous Equations for 4 Layers

A_1	C_1	A_2	C_2	A_3	C_3	A_4	C_4	RIGHT HAND SIDE
$1-(1-\epsilon)R_1$	$1-(1-\epsilon)\frac{1}{R_1}$	0	0	0	0	0	0	$\epsilon(B_0 - B_1)$
$e^{-\gamma_1 Z_1}$	$e^{\gamma_1 Z_1}$	$-e^{-\gamma_2 Z_1}$	$-e^{\gamma_2 Z_1}$	0	0	0	0	$B_2 - B_1$
$R_1 e^{-\gamma_1 Z_1}$	$\frac{1}{R_1} e^{\gamma_1 Z_1}$	$-R_2 e^{-\gamma_2 Z_1}$	$-\frac{1}{R_2} e^{\gamma_2 Z_1}$	0	0	0	0	$B_2 - B_1$
0	0	$e^{-\gamma_2 Z_2}$	$e^{\gamma_2 Z_2}$	$-e^{-\gamma_3 Z_2}$	$-e^{\gamma_3 Z_2}$	0	0	$B_3 - B_2$
0	0	$R_2 e^{-\gamma_2 Z_2}$	$\frac{1}{R_2} e^{\gamma_2 Z_2}$	$-R_3 e^{-\gamma_3 Z_2}$	$-\frac{1}{R_3} e^{\gamma_3 Z_2}$	0	0	$B_3 - B_2$
0	0	0	0	$e^{-\gamma_3 Z_3}$	$e^{\gamma_3 Z_3}$	$-e^{-\gamma_4 Z_3}$	$-e^{\gamma_4 Z_3}$	$B_4 - B_3$
0	0	0	0	$R_3 e^{-\gamma_3 Z_3}$	$\frac{1}{R_3} e^{\gamma_3 Z_3}$	$-R_4 e^{-\gamma_4 Z_3}$	$-\frac{1}{R_4} e^{\gamma_4 Z_3}$	$B_4 - B_3$
0	0	0	0	0	0	$R_4 e^{-\gamma_4 Z_4}$	$\frac{1}{R_4} e^{\gamma_4 Z_4}$	$-B_4$

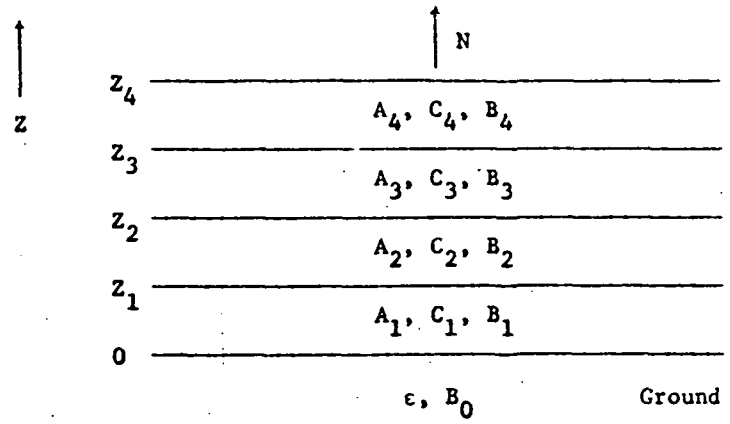

Figure 10

The outgoing flux density at the top of the cloud is obtained from the condition of continuity of I at this interface, which is

$$N = A_4 e^{-\gamma_4 Z_4} + C_4 e^{\gamma_4 Z_4} + B_4 \tag{23}$$

For a given experimental situation B(Z) and $K_g(Z)$ from Equation (20) are known. For any choice of K_p and S for the cloud of particles one can therefore obtain R(Z) and $\gamma(Z)$ from S and $K = K_g + K_p$. Then, with a suitable assumed value of ε, all coefficients in Table 6 are known so that A_4 and C_4 can be calculated by Gaussian elimination. A theoretical value of N can therefore be found from (23) for the particular choice of K_p and S. The same can be done for an experimental run with a widely different temperature profile, yielding a theoretical value N'. One then manipulates K_p and S until the theoretical values of N and N' agree with the measured values. Instead of the two-dimensional Newton's method, which is often troublesome, we prefer an iterative method with over-relaxation to carry out the computation.

The question of how large a difference in temperature profile is required to give good values of $K_p(\nu)$ and $S(\nu)$, free of the effects of temperature gradient and gas absorption, is best answered by actual trial on the computer. For this purpose one could plot a K_p versus S curve corresponding to matching of theoretical and experimental values of N for each temperature profile. Each of these curves can be obtained by Newton's method in one dimension. The intersection of the curves determines the required values of K_p and S. The accuracy of the procedure can be evaluated from the crossing angle of the two curves.

D. DETERMINATION OF $K(\nu)$ AND H WHEN $S(\nu)$ IS SMALL

We now restate the problem as being to find both the absorption coefficient $K_p(\nu)$ and the scale-height H of the particulate layer given two measured radiance spectra for widely different, but known, temperature profiles and a known profile of the gas absorption coefficient $K_g(\nu)$. Again we have two equations and two unknowns. The equations can be derived as follows.

In the absence of scattering the upward and downward radiative fluxes, I and J are given by the differential equations:

$$\frac{dI}{dZ} = -KI + KB \tag{24}$$

$$-\frac{dJ}{dZ} = -KJ + KB \tag{25}$$

where B is the Planck function and $K = K_g + K_p$ is the total absorption coefficient at any height Z. Since these equations are not coupled (on the assumption that the ground is black) and we are interested only in the upwards flux, Equation (25) may be disregarded. For a set of n layers, each with uniform K and B, the solution of (24) is:

$$I_1 = A_1 e^{-K Z} + B_1 \qquad (26)$$

$$I_2 = A_2 e^{-K_2 Z} + B_2$$

- - - - - - - - - -

$$I_n = A_n e^{-K_n Z} + B_n$$

At $Z = 0$, $I_1 = B_0$ where B_0 is the Planck function for the ground temperature. At $Z = Z_1$ the boundary between the first and second layer, $I_1 = I_2$, etc. Therefore:

$$A_1 = B_0 - B_1 \qquad (27)$$

$$e^{-K_1 Z_1} A_1 - e^{-K_2 K_1} A_2 = B_2 - B_1$$

$$e^{-K_2 Z_2} A_2 - e^{-K_3 Z_2} A_3 = B_3 - B_2$$

$$e^{-K_3 Z_3} A_3 - e^{-K_4 Z_3} A_4 = B_4 - B_3$$

- - - - - - - - - - - - - - - -

$$e^{-K_{n-1} Z_{n-1}} A_{n-1} - e^{-K_n Z_{n-1}} A_n = - B_n$$

The radiance from the top of the cloud is given by:

$$N = A_n e^{-K_n Z_n} + B_n \qquad (28)$$

For given values of the Ks, Zs and Bs, the set of Equations (27) can readily be solved sequentially for the unknown A's, starting at the first equation. In this way, A_n can be computed, and therefore N from Equation

In order to avoid overflow problems in the computer program, we replace A_1, A_2, ... by X_1, X_2, ..., where

$$X_1 = e^{-K_4 Z_4} A_1 \tag{29}$$

$$X_2 = e^{-K_4 Z_4} A_2$$

- - - - - - - -

Then (27) and (28) become

$$X_1 = e^{-K_4 Z_4}(B_0 - B_1) \tag{30}$$

$$X_2 = e^{-(K_2 - K_1)Z_1} X_1 - e^{K_2 Z_1 - K_4 Z_4}(B_2 - B_1)$$

- -

and

$$N = X_n + B_n \tag{31}$$

As a preliminary step in the computer program we have chosen to compress the atmosphere in such a way that the exponentially distributed dust with assumed scale height H becomes a layer of uniform density extending from the ground to a height H. The required transformation is:

$$Z' = H\left(1 - e^{-Z/H}\right) \tag{32}$$

where Z is transformed into Z'. The same transformation is, of course, applied to the atmospheric gas. The experimentally determined temperatures T(Z) are kept constant in the transformation, i.e.:

$$T(Z') = T(Z) \tag{33}$$

The known absorption coefficient $K_g(Z)$ of the gas is transformed according to the relation

$$K_g(Z') = \frac{K_g(Z)}{dZ'/dZ} = K_g(Z)e^{Z/H} \qquad (34)$$

In the computer program, for the first temperature profile at a given frequency, we select a value of the dust scale height H and then by Newton's method find what value of the dust absorption coefficient K_p gives a theoretical radiance in agreement with the experimental value at the chosen frequency. This is repeated for a series of values of H, so that a graph of K_p versus H can be drawn from the computer output. The same is done for the other temperature profile. The intersection of the two K_p versus H graphs gives the solution for dust scale height and the absorption coefficient at the chosen frequency. On repeating the procedure at another frequency a different value of K_p will, in general, be found but H should, of course, be the same if the experimental data are noise-free and free of systematic error.

On running the program for morning and afternoon temperature profiles at a frequency of 1000 cm^{-1}, for which the atmospheric absorption is very weak, we found that the two computed K_p versus H curves crossed each other at an angle of about 90° (Figure 11) and yielded the solution $H = 7$ km and $K_p = 1.1 \times 10^{-6}$ cm^{-1}. The value of H is in fair agreement with the scale height of about 10 km for the Martian atmosphere. The optical thickness K_pH of the dust cloud at this frequency is 0.77.

Unfortunately, on repeating the computations at 506 cm^{-1} (Figure 12), we found that the K_p versus H curve for the morning profile stayed above the curve for the afternoon profile for all values of H. Therefore, no solution could be obtained. The reason for this difficulty is that the morning temperature profile is too close to isothermal to provide much information about the dust cloud. If the profile were strictly isothermal, at the same temperature as the ground, the observed radiance would have a blackbody spectrum corresponding to the ground temperature and would therefore contain no information about $K_p(\nu)$ or H.

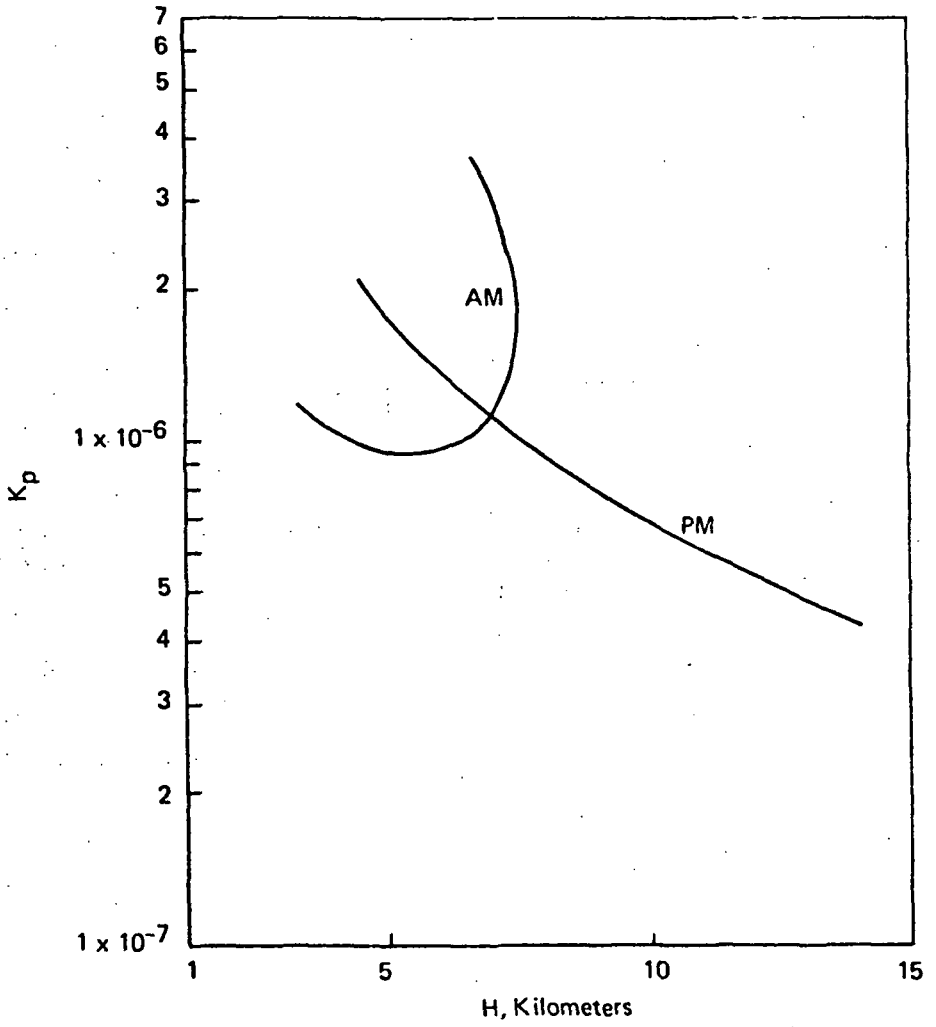

FIGURE 11 1,000 cm^{-1} K_p VS H CURVES

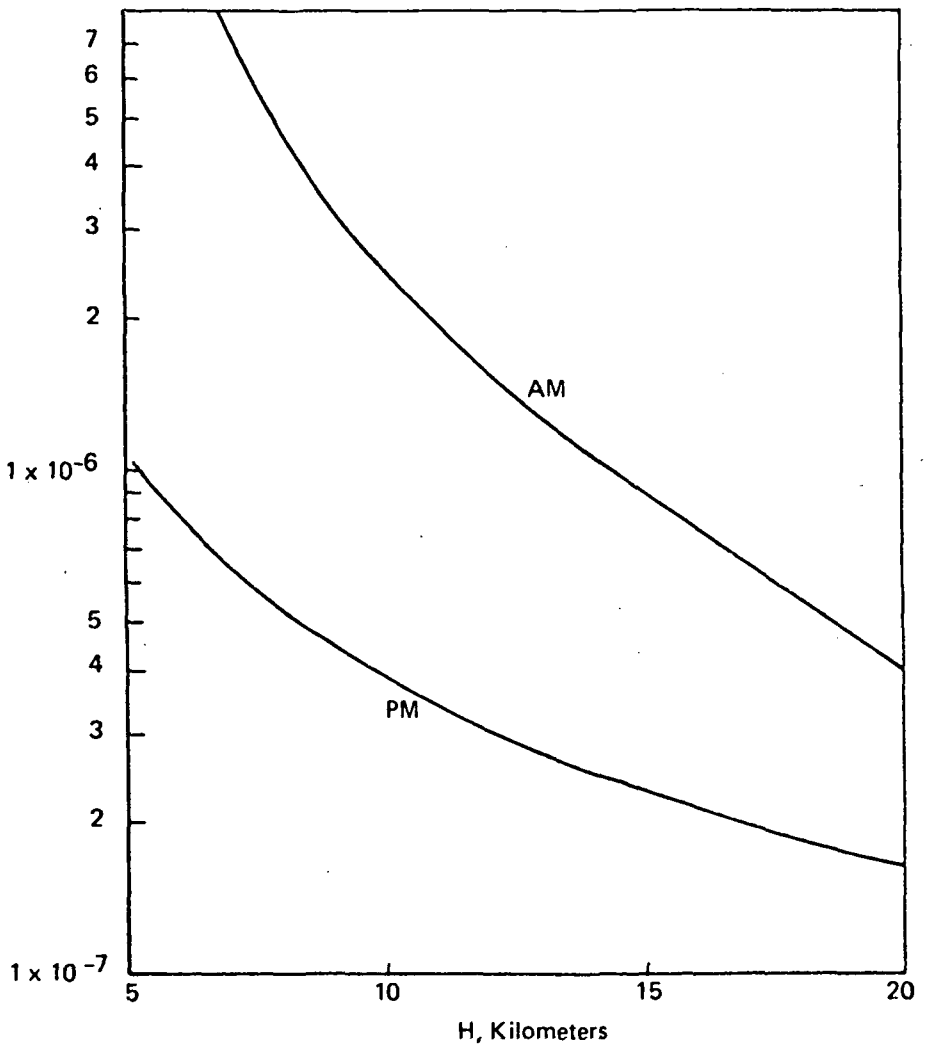

FIGURE 12 506 cm^{-1} K_p VS H CURVES

To investigate the question further, we have examined the behavior of N versus K_p for the various cases. When the temperature varies monotonically with height (including the ground temperature) N versus K_p is a steep curve that intersects the experimental N at a well defined value of K_p. On the other hand, when the Planck function for the ground is between the Planck functions for the various layers (morning profile), the curve is quite flat and K_p is very susceptible to small errors in the experimental radiance.

We believe that the procedure for determining K_p and H would work very well if the second profile were monotonically increasing with height or monotonically decreasing at a significantly lower rate than for the afternoon profile. We recommend that NASA should search for such a pair of profiles and carry out the necessary computations with the help of our program.

We also recommend, if a suitable second profile is not available, that the data for the afternoon profile should be used alone, along with an assumed value of dust scale height, e.g., 10 km, to determine a complete K_p spectrum. Such a spectrum will be free of the effects of the temperature distribution and of atmospheric absorption and will be equivalent to the transmission spectrum (without reflection losses) obtained by a laboratory spectrometer for a single crystal of the dust material. Such a presentation of the Martian infrared data would allow simple averaging of K_p over many spectra for purposes of comparison with laboratory transmission spectra of various candidate minerals.

E. COMPUTER PROGRAMS

A listing of MARK, the computer program we wrote to carry out the inversion when S = 0 is given in Figure 13. This program was written in double precision fortran for the General Electric Mark III Time Sharing Service.

```
MARK         11:03EDT    09/27/74

100C   UP TO 50 LAYERS
110    IMPLICIT DOUBLE PRECISION (A-H)
120    IMPLICIT DOUBLE PRECISION (O-Z)
130    DIMENSION T(50),P(50),ALP(50),Z(50),TEMP(5),AA(50)
140   &,CAPK(50),ZSQ(50)
145   REAL TEMP,DX,PIP,ZR
150    BPL(TE)=1.1909D-12*WN*WN*WN/(DEXP(1.438D0*WN/TE)-1.D0)
160    ITER=1
170  1 PRINT,"READ IN WN,AVGRAD,N,H,E,TG,ALPH,PS,TS"
180    READ("NUM3",999)WN,AVGRAD,N H,EM,TG,ALPH,(P(I),T(I),I=1,N)
185 999 FORMAT(V)
190    PRINT,WN,AVGRAD,N,H,EM,TG,ALPH,(P(I),T(I),I=1,N)
200    CAPI=1.D-5
205    ALPH=10.D0**ALPH
210C   TRANSFORM P TO Z
220C    PO IS AT THE GROUND
230    RGAS=1.8892D6
232    PCONV=9.8693D-4
234    DO 10 I=1,N
236 10 P(I)=P(I)*PCONV
237    NI=N-1
238    DO 11 I=1,NI
240 11 ALP(I)=ALPH*15.D0*(P(I)+P(I+1))/(2.D0*DSQRT((T(I)+T(I+1))/2.D0))
241    GMARS=376.D0
260    DO 60 I=1,NI
261    IZ=0
262    DO 70 IN=1,5
263 70 TEMP(IN)=0.
264    DDX=0.D0
265    DPIP=T(1)/P(1)
266 65 CONTINUE
267    DX=DDX
268    PIP=DPIP
269    ZR=CLCINT(1,DX,PIP,TEMP)
270    Z(1)=-RGAS*DBLE(ZR)/GMARS
271    IZ=IZ+1
272    IF(IZ.GE.N) GO TO 51
273    DDX=P(IZ+1)-P(IZ)
274    DPIP=(T(IZ)+T(IZ+1))/(P(IZ)+P(IZ+1))
275    IF(I.GE.IZ) GO TO 65
276 60 CONTINUE
280 51 IST=0
290    DEK=.005D0*CAPI
300    CAPKD=CAPI-DEK
310 25 CONTINUE
340    DO 2 I=1,NI
350    IF(ITER.GT.1) GO TO 53
360    IF(IST.GE.1) GO TO 53
380    ZSQ(I)=H*(1.D0-DEXP(-Z(I)/H))
395 53 CAPKG=1.732051D0*ALP(I)*DEXP(Z(I)/H)
400 55 CAPK(I)=CAPKG*CAPKD
410  2 CONTINUE
415   CONS=CAPK(NI)*ZSQ(NI)
420    AA(1)=(EPL(TG)-BPL(T(1)))*DEXP(-CONS)
430    DO 90 I=2,NI
440    AA(I)=AA(I-1)*DEXP(ZSQ(I-1 )*(CAPK(I)-CAPK(I-1)))-DEXP
450   &(ZSQ(I-1)*CAPK(I)-CONS)*(BPL(T(I))-BPL(T(I-1)))
460 90 CONTINUE
470    RAD=AA(NI)*BPL(T(NI))
475  PRINT,RAD
480    IF(IST.EQ.1) GO TO 22
490   DEL=RAD-AVGRAD
500    CAPKD=CAPKD+2.D0*DEK
510    IST=IST+1
520    GO TO 25
530 22 DELK=RAD-AVGRAD
540   DFDK=(DELK-DEL)/(2.D0*DEK)
550   CAPI=CAPI-(DEL+DELK)/(2.D0*DFDK)
570   PRINT,ITER,CAPI
580  ITER=ITER+1
590   GO TO 51
600   END
```

FIGURE 13

It can be rather simply converted to any other fortran service by suitable changes in the I/O statements and replacement or deletion of the integration subroutine CLCINT. This subroutine is used to calculate the equivalent heights Z(i) for the various layers, i, from the pressure and temperature data if the number of layers used is less than the total number given. It is a modified Simpson's rule integration. The calling sequence is ZR = CLCINT (1, DX, PIP, TEMP). 1 is an indicator for the modified Simpson's rule, DX is set equal to 0 for the initial call and to the desired increment thereafter, PIP is the integrand and TEMP is a storage array.

Appendix

General Description of Fitting Process

The first step we take is to read the graphical output of the spectrometer at intervals of 5-10 cm^{-1} and enter the data in digital form into a time-sharing system. After performing a linear transformation to correct for the zero and one-hundred percent reflectance errors, we make a new graph of the data on a Hewlett-Packard 7200A plotter which is attached to the terminal used to access the time-sharing system. Transcription errors and doubtful data points are easily pinpointed and eliminated at this juncture. We then make a final plot of the purified data; reproductions of this plot are used later to assist in the fitting process. The purified data are also listed and punched in cards to serve as input to the program used to carry out the least squares fitting.

Our regression (least square fitting) program requires that first approximations to the Lorentz line parameters be supplied as input. We make use of the HP plotter and time-sharing system to help obtain the required first guesses by plotting the reflection spectrum corresponding to the guessed Lorentz lines on reproductions of the data plot. It is fairly easy to adjust the parameters to ameliorate a grossly erroneous approximation. After two or three lines have been roughly established in a limited band at, say, the high frequency end of the spectrum, we improve the fit by means of the least squares program. Then we make a graph of the results and guess the parameters for a few more lines to expand the range of frequencies covered; again the entire set is improved by the least squares fitting program. In this way the full span of the spectral data is eventually covered. We find that this stepwise procedure needs much less mental and computational effort than an attempt to guess ten to fifteen lines simultaneously to start the fitting process.

The Regression Problem and Method of Solution

We are given the spectral reflectance of a sample as measured by a known instrument and we wish to find the values of a set of classical oscillator parameters that give the theoretical reflectance spectrum that best matches the measured spectrum. We solve the problem by the method of least squares; that is, we vary the oscillator parameters to minimize the root mean square difference between the measured and theoretical spectra.

Let R_j be the reflectance measured at a frequency ν_j and $R(\nu,P)$ be the theoretical reflectance of a sample with the set of oscillator parameters P at a frequency ν. We wish to minimize the residual

$$T = \sum_j (R(\nu_j,P) - R_j)^2 \qquad (A1)$$

which we can do by setting equal to zero the partial derivatives of T with respect to the individual parameters. Due to the complicated nature of the function $R(\nu,P)$, however, the resulting simultaneous equations are highly non-linear and must be solved iteratively.

The function $R(\nu,P)$ may be broken into two parts corresponding to the two planes of polarization π and s which are parallel and perpendicular, respectively, to the plane of incidence of the beam of light falling on the sample in the measuring instrument. We write

$$R(\nu,P) = a_\pi(\nu)\, R_\pi(\nu,P) + a_s(\nu)\, R_s(\nu,P) \qquad (A2)$$

where $a_\pi(\nu)$ and $a_s(\nu)$ are instrumental corrections taken to be known functions of frequency.

The Fresnel formulas give $R_\pi(\nu,P)$ and $R_s(\nu,P)$ in terms of the angle of incidence ϕ and dielectric constant $\varepsilon = \varepsilon(\nu,P)$ which characterizes the electrical properties of the material. Thus

$$R_\pi = |r_\pi|^2 \qquad (A3)$$

$$R_s = |r_s|^2 \qquad (A4)$$

$$r_\pi = \frac{\varepsilon \cos\phi - Z}{\varepsilon \cos\phi + Z} \tag{A5}$$

$$r_s = \frac{Z - \cos\phi}{Z + \cos\phi} \tag{A6}$$

$$Z = \sqrt{\varepsilon - \sin^2\phi} \tag{A7}$$

Finally, according to classical dispersion theory, the dielectric constant has the form of a sum of m simple resonances (Lorentz lines):

$$\varepsilon(\nu,P) = \varepsilon_o + \sum_{k=1}^{m} \frac{S_k}{1 + i\,\gamma_k \frac{\nu}{\nu_k} - \left(\frac{\nu}{\nu_k}\right)^2} \tag{A8}$$

In our work, we take the set of parameters P to be made up of the following quantities:

$$p_{oo} = \varepsilon_o \tag{A9}$$

$$p_{1k} = S_k \tag{A10}$$

$$p_{2k} = \frac{\gamma_k}{\nu_k} \tag{A11}$$

$$p_{3k} = \frac{1}{\nu_k^2} \tag{A12}$$

Thus the equations to be solved simultaneously for the parameters $p_{\mu k}$ are seen to be

$$\frac{\partial T}{\partial p_{\mu k}} = 0 \tag{A13}$$

whence, by Equation A1, we find

$$\sum_j \left[R(\nu_j,P) - R_j\right] \frac{\partial R(\nu_j,P)}{\partial p_{\mu k}} = 0 \tag{A14}$$

It is evident that the quantities r_π and r_s (which are amplitude ratios) are analytic functions of the parameters $p_{\mu k}$, but that the intensity ratios R_π, R_s and R are not, and therefore the calculation of their derivatives requires some special medicine in the form of a simple lemma, to wit:

Let $w(z)$ be an analytic function of $z = x + iy$. Then it is easy to show that

$$\frac{\partial |w|^2}{\partial x} = 2\,\mathrm{Re}\left(w^* \frac{dw}{dz}\right), \tag{A15}$$

the asterisk denoting the complex conjugate.

We see that

$$\frac{\partial R(\nu,P)}{\partial p_{\mu k}} = 2a_\pi(\nu)\,\mathrm{Re}\left(r_\pi^* \frac{\partial r_\pi}{\partial p_{\mu k}}\right) + 2\,a_s(\nu)\,\mathrm{Re}\left(r_s^* \frac{\partial r_s}{\partial p_{\mu k}}\right) \tag{A16}$$

The differentiations called for in Equation A16 are elementary; the work is simplified by use of the relations

$$\frac{\partial r_\pi}{\partial p_{\mu k}} = \frac{dr_\pi}{d\epsilon}\,\frac{\partial \epsilon}{\partial p_{\mu k}} \tag{A17}$$

and

$$\frac{\partial r_s}{\partial p_{\mu k}} = \frac{dr_s}{d\epsilon}\,\frac{\partial \epsilon}{\partial p_{\mu k}} \tag{A18}$$

We find

$$\frac{dr_\pi}{d\epsilon} = \frac{\cos\phi}{Z}\,\frac{\epsilon - 2\sin^2\phi}{(\epsilon\cos\phi + Z)^2} \tag{A19}$$

$$\frac{dr_s}{d\epsilon} = \frac{\cos\phi}{Z}\,\frac{1}{(Z + \cos\phi)^2} \tag{A20}$$

and

$$\frac{\partial \epsilon}{\partial p_{oo}} = 1 \tag{A21}$$

$$\frac{\partial \epsilon}{\partial p_{1k}} = \frac{1}{D_k} \tag{A22}$$

$$\frac{\partial \epsilon}{\partial p_{2k}} = \frac{-i\nu}{D_k^2} \tag{A23}$$

$$\frac{\partial \epsilon}{\partial p_{3k}} = \frac{\nu^2}{D_k^2} \tag{A24}$$

where we have written, for short,

$$D_k = 1 + i\, p_{2k}\nu - p_{3k}\nu^2. \qquad \text{(A25)}$$

Equations A16 through A25 suggest clearly the few lines of Fortran coding needed to compute the derivatives which occur in Equation A14. If the coding is systematically organized, the machine time needed to compute all the required derivatives is not great in comparison to the computation of $R(\nu,P)$ itself.

The next question to be discussed is the numerical method used for solving the set of simultaneous equations of the type of Equation A14. In the past, we have used Gauss-Seidel iteration with over-relaxation, solving the individual equations by Newton's method. However, we were plagued with frequent divergences, lines whose resonance frequencies wandered excessively, lines coalescing with neighbors, and so on. Others[19] have used the method of steepest descent at first, followed by Newton's method as a final phase. The objection to the descent method, perhaps only philosophical, is that the distance traveled in the steepest direction must at the same time have conflicting units ascribed to it. To put it another way, if the units in which the problem is stated are changed, the sequence of steps in the descent process will suffer a change which is of a substantial nature.

It is also preferable, in automatic computation, to use a unified procedure rather than a sequence of two or more procedures, which entails the decision of when to move from one phase to the next to be made, as well as the chore of extra coding.

In our recent work, reported on here, we have employed a different technique which is a hybrid between Newton's method and descent methods. What we do is to calculate a certain approximation δP to the correction to all the parameters P as prescribed by Newton's method but then make only the correction $c\,\delta P$, where c is a scalar selected to minimize the residual. In the usual form of Newton's method, a set of simultaneous linear equations must be solved or, equivalently, a matrix must be

inverted. When the starting approximation is poor, the matrix may be singular or nearly so, and difficulties in solving the equations and instabilities are commonly experienced. In our method, we take a matrix which is an approximation to the matrix occurring in Newton's method but which is positive definite, so that inversion is always possible.

To elucidate the method mathematically we will eliminate the double subscripts μ and k used hitherto to distinguish the parameters by setting

$$p_\ell = p_{\mu k} \tag{A26}$$

with $\ell = 0$ for $\mu = k = 0$

$\ell = 3(k - 1) + \mu$ for $\mu, k \geq 1$

Using this notation we may write the simultaneous equations to be solved (Equation A14) in the form

$$\sum_j [R(\nu_j,P) - R_j] \frac{\partial R(\nu_j,P)}{\partial p_\ell} = 0 \tag{A27}$$

Now suppose that we have an approximation P_o to the set of parameters P. We substitute P_o for P in Equation A27; of course, the right-hand side will not be zero but some other quantity, say δT_ℓ. Thus

$$\sum_j [R(\nu_j,P_o) - R_j] \frac{\partial R(\nu_j,P_o)}{\partial p_\ell} = \delta T_\ell \tag{A28}$$

Now let the error in P_o be δP. We substitute the expression

$$P = P_o - \delta P \tag{A29}$$

into Equation A27 and expand in power series, keeping only the first order terms, to find

$$\sum_\lambda \sum_j \left\{ \frac{\partial R(\nu_j,P_o)}{\partial p_\ell} \frac{\partial R(\nu_j,P_o)}{\partial p_\lambda} + [R(\nu_j,P_o)-R_j] \frac{\partial^2 R(\nu_j,P_o)}{\partial p_\ell \partial p_\lambda} \right\} \delta p_\lambda = \delta T_\ell \tag{A30}$$

Equation A30 represents a set of linear simultaneous equations to be solved for the errors δp_λ and is the mathematical expression of Newton's method. In our procedure we drop the second term, $[R(\nu_j,P_o) - R_j] \frac{\partial^2 R(\nu_j,P_o)}{\partial p_\ell \, \partial p_\lambda}$, in the coefficient of δp_λ for two reasons. First of all, when P_o is close to P, the theoretical spectrum should be close to the measured spectrum, so the quantity $[R(\nu_j,P_o) - R_j]\, \delta p_\lambda$ is second order. In the second place, the matrix whose elements are $\sum_j \frac{\partial R(\nu_j,P_o)}{\partial p_\ell} \frac{\partial R(\nu_j,P_o)}{\partial p_\lambda}$ is positive definite and symmetric, and therefore its inverse is known to exist and is likely to be easy to compute. Therefore we set up and solve the equations

$$\sum_{\lambda} \sum_{j} \frac{\partial R(\nu_j,P_o)}{\partial p_\ell} \frac{\partial R(\nu_j,P_o)}{\partial p_\lambda} \delta p_\lambda = \delta T_\ell \qquad \text{(A31)}$$

Having found the elements δp_λ of the set δP from Equation A31, we next find the scalar c which minimizes the residual

$$T(c) = \sum_j [R(\nu_j,P_o - c\delta P) - R_j]^2 \qquad \text{(A32)}$$

We do this simply by tabulating T(c) at a few well chosen values of c and finding the minimum of an interpolating parabola. Once the new approximation $P_o - c\delta P$ is found the process is repeated until the residual converges to some irreducible value, whereupon the last approximation to the set of parameters is declared to be the required set.

Statistical Analysis

Once the Lorentz line parameters themselves are determined it is desirable to estimate their standard deviations to get an idea of the errors that may be in the parameters determined by the least squares fit. To do this we make the assumption that the difference between the theoretical and measured spectra is entirely unsystematic and due only to noise which is uniform over the spectrum. This may be well warranted in some cases but it is not entirely valid in others, and therefore the

results of the statistical analysis may not be quantitatively correct. The statistical estimates of error should, however, serve to indicate which parameters are better or worse determined than others in the same spectrum. In any case, this basic assumption should always be borne in mind when one is interpreting the estimates of standard deviations.

In order to calculate the standard deviations of the Lorentz line parameters we imagine the measurements R_j to be in error by amounts δR_j and calculate the change, δP, that this causes in the parameters that result from the least squares fit. Evidently the equations to be satisfied are

$$\sum_j [R(\nu_j, P + \delta P) - R_j - \delta R_j] \frac{\partial R(\nu_j, P + \delta P)}{\partial p_\ell} = 0 \qquad \text{(A33)}$$

Now we expand Equation A33 in the manner used to expand Equation A28 and again neglect all but the lowest order terms to obtain a set of simultaneous linear equations for the errors δp_λ in the parameters:

$$\sum_\lambda \sum_j \frac{\partial R(\nu_j, P)}{\partial p_\ell} \frac{\partial R(\nu_j, P)}{\partial p_\lambda} \delta p_\lambda = \sum_j \frac{\partial R(\nu_j, P)}{\partial p_\ell} \delta R_j \qquad \text{(A34)}$$

Equation A34 may be written in matrix notation as

$$UU^T \delta P = U\delta R \qquad \text{(A35)}$$

where U is a matrix whose elements are

$$u_{\ell j} = \frac{\partial R(\nu_j, P)}{\partial p_\ell}$$

δR is the vector whose elements are δR_j
the superscript T denotes transpose.

The matrix UU^T is the symmetric, positive definite matrix encountered previously in the discussion of the descent method.

Clearly, we cannot solve Equation A35 for δP since we have no way of knowing δR, but we can obtain statistical information about δP. To start with we take the expectations (symbolized by the angle brackets) of both

sides of Equation A35:

$$UU^T \langle \delta P \rangle = U \langle \delta R \rangle \tag{A36}$$

Obviously, if $\langle \delta R \rangle = 0$, as we have a right to assume it is, then it follows that $\langle \delta P \rangle = 0$. In other words, if the measurements are unbiased, then the estimates of the parameters are unbiased. To get a second moment we multiply both sides of Equation A35 by their transposes and take the expectation of the result. We may write

$$UU^T \langle \delta P \delta P^T \rangle \quad UU^T = U \langle \delta R \delta R^T \rangle \quad U^T \tag{A37}$$

We assume now that the measurement errors are independent and all have the same standard deviation σ. Thus the matrix $\langle \delta R \delta R^T \rangle$ is a diagonal matrix with diagonal elements all equal to σ^2 and Equation A37 becomes

$$UU^T \langle \delta P \delta P^T \rangle \quad UU^T = UU^T \sigma^2 \tag{A38}$$

whence the matrix of variances and covariances of the Lorentz line parameters is seen to be

$$\langle \delta P \delta P^T \rangle = (UU^T)^{-1} \sigma^2 \tag{A39}$$

An estimate of σ^2 may be obtained from the residual after the least squares fit. We take

$$\sigma^2 = \frac{\sum_j [R(\nu_j, P) - R_j]^2}{N - 3m - 1} \tag{A40}$$

where N is the number of measurements made

m is the number of Lorentz lines used for fitting

Finally it is to be noted that the variances of the classical oscillator parameters ϵ_o, S_k, γ_k and ν_k are related to the elements of the variance matrix computed according to Equation A39 by the relations

$$\langle \delta \epsilon_o^2 \rangle = \langle \delta p_{oo}^2 \rangle \tag{A41}$$

$$\langle \delta S_k^2 \rangle = \langle \delta p_{1k}^2 \rangle \tag{A42}$$

$$\langle \delta\gamma_k^2 \rangle = \langle \delta p_{2k}^2 \rangle - p_{2k} p_{3k}^{-\frac{3}{2}} \langle \delta p_{2k} \delta p_{3k} \rangle + \frac{1}{4} p_{3k}^{-3} \langle \delta p_{3k}^2 \rangle \qquad \text{(A43)}$$

$$\langle \delta\nu_k^2 \rangle = \frac{1}{4} p_{3k}^{-3} \langle \delta p_{3k}^2 \rangle \qquad \text{(A44)}$$

REFERENCES

1. B. Conrath, R. Curran, R. Hanel, V. Kunde, W. Maguire, J. Pearl, J. Pirraglia and J. Welker, J. Geophys. Res. 78, 4267 (1973).

2. R. Hanel, B. Conrath, W. Hovis, V. Kunde, P. Lowman, W. Maguire, J. Pearl, J. Pirraglia, C. Prabhakara, B. Schlachman, G. Levin, P. Straat and T. Burke, Icarus 17, 423 (1972).

3. G. R. Hunt, L. M. Logan and J. W. Salisbury, Icarus 18, 459 (1973).

4. E. E. Angino, Nature 204, 569 (1964).

5. H. Moenke, "Mineralspektren," Academie-Verlag, Berlin, 1962.

6. V. Stubican and R. Roy, Am. Mineral. 46, 32 (1961).

7. A. G. Emslie and J. R. Aronson, Appl. Opt. 12, 2563 (1973).

8. J. R. Aronson and A. G. Emslie, Appl. Opt. 12, 2573 (1973).

9. J. R. Aronson and A. G. Emslie, in "Infrared and Raman Spectroscopy of Lunar and Terrestrial Minerals," Academic Press, 1974, in press.

10. H. C. van de Hulst, "Light Scattering by Small Particles," Wiley, New York, 1957.

11. J. E. Conel, J. Geophys. Res. 74, 1614 (1969).

12. W. G. Spitzer and D. A. Kleinman, Phys. Rev. 121, 1324 (1961).

13. J. B. Pollack, D. B. Toon and B. N. Khare, Icarus 19, 372 (1973).

14. P. J. Launer, Am. Mineral. 37, 764 (1952).

15. W. Vedder, Am. Mineral. 49, 736 (1964).

16. J. R. Aronson, A. G. Emslie, L. H. Roach, P. F. Strong and P. C. von Thüna, Development of a Theory of the Spectral Reflectance of Minerals, Part II, Report on NAS9-10875 (April 1, 1971).

17. R. J. P. Lyon, NASA Technical Note D-1871, 1963.

18. V. C. Farmer and J. D. Russell, Spectrochim. Acta 20, 1149 (1964).

19. H. W. Verleur, J. Opt. Soc. Am. 58, 1356 (1968).

END

DATE

FILMED

JUN 19 1975